Journal of Biological Systems, Vol. 8, No. 2 (2000) 115–139

ENERGY ANALYSIS OF A NONLINEAR MODEL OF THE NORMAL HUMAN LUNG

A. ATHANASIADES*, F. GHORBEL*,¶, J. W. CLARK Jr.*,†, S. C. NIRANJAN*,†,‡, J. OLANSEN*, J. B. ZWISCHENBERGER†,§ and A. BIDANI†,‡

Dynamical Systems Group, School of Engineering, Rice University, Houston, TX 77005, USA*
Biomedical Engineering Center†, Departments of Internal Medicine‡ and Thoracic Surgery§, University of Texas Medical Branch, Galveston, TX 77555, USA

Accepted 13 May 1999

ABSTRACT

Despite the existence of respiratory mechanics models in the literature, rarely one finds analytical expressions that predict the work of breathing (WOB) associated with natural breathing maneuvers in non-ventilated subjects. In the present study, we develop relations that explicitly identify WOB, based on a proposed nonlinear model of respiratory mechanics. The model partitions airways resistance into three components (upper, middle and small), includes a collapsible airways segment, a viscoelastic element describing lung tissue dynamics and a static chest wall compliance. The individual contribution of these respiratory components on WOB is identified and analyzed. For instance, according to model predictions, during the forced vital capacity (FVC) maneuver, most of the work is expended against dissipative forces, mainly during expiration. In addition, expiratory dissipative work during FVC is almost equally partitioned among the upper airways and the collapsible airways resistances. The former expends work at the beginning of expiration, the latter at the end of expiration. The contribution of the peripheral airways is small. Our predictions are validated against laboratory data collected from volunteer subjects and using the esophageal catheter balloon technique.

Keywords: Work of breathing, respiratory mechanics, viscoelasticity, Campbell diagram.

1. Introduction

The term *work of breathing* (WOB) refers to the work performed by the respiratory muscles during breathing. This work is done mainly against three groups of forces [25]: (a) elastic forces developed in the tissues of the lung and chest when a volume change occurs; (b) dissipative forces caused by the resistance in the airways (flow-resistive) and by the viscoelastic deformation of tissue; (c) inertial forces, depending on the mass of tissue and gases. Based on this classification, and in direct correspondence to the terminology employed in this study, the work can be partitioned among elastic, dissipative, or inertial (usually considered negligible) components.

¶Author for correspondence: Department of Mechanical Engineering, Mailstop 321, Rice University, 6100 Main Street, Houston, Texas 77005. E-mail: ghorbel@rice.edu

Instrumentation and methodologies developed for the measurement of WOB rely on simultaneous pleural pressure and lung volume recordings. The former is approximated by esophageal pressure, measured with a naso-gastric catheter balloon [21]. Volume is measured either with spirography or by integrating volumetric flow from a pneumotachograph. In clinical practice, the two variables (pressure and volume) are directed to a computerized monitor and plotted against each other. In this manner, work is estimated by calculating the area enclosed in the pleural pressure loop [1].

WOB measurement finds application in the assessment of respiratory failure and in ventilatory management, as an indicator of the metabolic energy of breathing. Although the energy required for quiet breathing is small (only 1-2% of total oxygen consumption), during exercise this amount can increase considerably (up to 10%) [13]. Subjects suffering from obstructive pulmonary disease require greater energy to breathe than healthy subjects [12,25]. Recently, with the advent of new ventilatory modes for the critically ill patient, assessment of breathing effort has received revived interest among clinicians. WOB is used as an index to: (a) monitor respiratory muscle fatigue or atrophy [17]; (b) to unload respiratory muscles [5,6]; (c) as a weaning index in terminating ventilatory support [2]; and (d) to regulate partial ventilatory support [3].

Recent research on the work of breathing has mostly been of clinical nature, focusing on either the clinical implications of WOB, especially in the assessment of the benefit of ventilatory assistance [2,3,5,6], or on the improvement of methodologies and instrumentation required for the accurate recording of muscular effort [4,7]. Apart from the early work of Otis *et al.* [24,25,26], little has been done to establish the theoretical underpinning of WOB. Although models of the pulmonary system have been developed [10,16,23,32], to our knowledge none has included a companion study of WOB.

Our objective in this paper is to gain better insight into the energetics of normal respiratory function. Past analyses have been limited in their contribution by assuming a linear, single compartment model of respiratory mechanics. We employ a model that includes nonlinear characterizations of airway resistance, chest wall compliance and lung tissue viscoelasticity. The model features separate resistive coefficients for the upper, middle and small airways; a compliant characterization of partially supported airways; a modified Kelvin body that describes the dynamic compliance of lung tissue; and a static compliance for the chest wall. We examine the contribution of these individual respiratory system components on the work of breathing at different breathing patterns. In particular, we investigate how changes in tidal volume and breathing frequency in breathing maneuvers affect WOB and its components. Our results are initially expressed mathematically, following a Lagrangian analysis of the respiratory model; subsequently they are analyzed in a graphical manner. Model predictions are validated against laboratory data collected from healthy human subjects.

2. Methods

2.1. *Experimental Measurement*

Experimental data were collected on four healthy human subjects (physiological parameters appear in Table 1) using a pneumotachograph and esophageal balloon ([15] includes a detailed description of the data collection procedure). Simultaneous measurements of pleural (esophageal) pressure and flow at the mouth were used to construct a pressure-volume (P-V) diagram, the volume derived from flow by integration. According to common clinical practice, we measured work of breathing (WOB) from the area formed in the P-V diagram, as illustrated later. Our model suggests methods that can lead to a more complete accounting of WOB, yet we have adopted this clinical techique in order to compare model predictions against an established standard. Chest wall elastic recoil, required to evaluate elastic work, is difficult to measure and was approximated, following common practice [29].

Table 1. Physical parameters for volunteer subjects.

subject no.	age, yr	height, in.	weight, lb.	FRC, liters	RV, liters	TLC, liters
1	34	70	185	2.42	1.24	5.19
2	39	72	165	4.54	2.04	8.27
3	38	66	161	3.04	1.61	6.34
4	40	72	180	2.78	1.91	7.20

FRC, functional residual capacity; RV, residual volume; TLC, total lung capacity. Volume and capacities determined from calculations implemented in body plehysmograph.

2.2. *Model Development of Respiratory Mechanics*

The mathematical model employed here is based on our respiratory model developed in [15]. A physical representation of the model, depicting its individual components, appears in Fig. 1A. To allow for a complete accounting of the work associated with breathing and for a better response to maneuvers of variable frequency, the following modifications are introduced to the original model:

(i) a nonlinear compliance C_{cw} is used to represent the combined elastic behavior of the chest wall and diaphragm, such that the energy stored in these structures can be accounted for;

(ii) as a result of this modification, the signal driving the model is no longer pleural pressure P_{pl}, but rather the pressure P_{mus}, which describes the net equivalent effect of respiratory muscle activity; P_{mus} is directly influenced by the repsiratory controller in the brain and its waveform is easily reproduced in simulated maneuvers; and

(iii) a viscoelastic structure (Kelvin body) replaces the original pressure-volume characterization of lung tissue. The modifications are treated in more detail below.

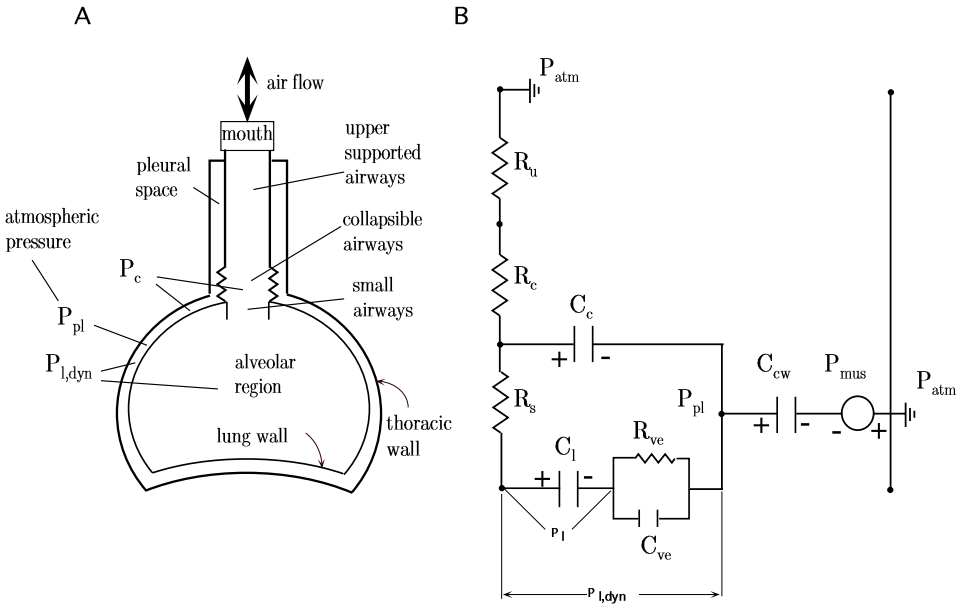

Fig. 1. A: Physical model of respiratory system (structure not drawn to scale, adapted from [15]); B: Pneumatic analog of model.

Model functions and parameters for all subjects are summarized in Tables 2 and 3, respectively. Parameter values of the full nonlinear model have been tuned to match experimental records of volume and flow in the FVC maneuver, as it is rich enough to excite most system dynamics. In general, parameter values comply with specifications given in [15]. In addition, they remain unchanged for all simulated maneuvers in a single subject.

2.2.1. *Chest Wall*

In our previous studies [15], the chest wall was assumed rigid and the lungs were driven by the pleural pressure waveform measured via the esophageal balloon technique. Since elastic forces developed in the chest wall and diaphragm expend part of the effort during breathing, we have reformulated our model to include a lumped characterization of the thoracic wall and diaphragm. They are modeled as a series combination of an independent pressure source, P_{mus}, serving as the dynamic force driving the model, and a passive compliant element, C_{cw}, as shown in Fig. 1B. The volume of air contained in C_{cw} is the chest wall volume, V_{CW}, and the pressure across it is the chest wall elastic recoil, P_{cw}; it equals the difference between the total pressure across the chest wall, pleural pressure P_{pl}, and the pressure developed due to the respiratory muscles,

$$P_{pl} = P_{cw} - P_{mus}\,. \tag{1}$$

P_{cw}, is commonly approximated by a sigmoidal curve [29], that is linear in the

Table 2. Model functions.

Respiratory muscle pressure	$P_{mus} = P_{cw} - P_{pl}$	for data comparisons*
	$= A_{mus} \cdot \sin(2\pi f t) + A_{mus}$	for simulations in Secs. 3.1 and 3.4 only
Chest wall elastic recoil	$P_{cw} = A_{cw} - B_{cw}\ ln\left(\frac{TLC-RV}{V_{CW}-RV} - 0.999\right)$	
Lung tissue static elastic recoil	$P_l = A_l\, e^{K_l \cdot V_A} + B_l$	
Collapsible airways elastic recoil	$P_c = A_c + B_c \left(\frac{V_C}{V_{C\,max}} - 0.7\right)^2$	if $\frac{V_C}{V_{C\,max}} \leq 0.5$
	$= 5.6 - B'_c \cdot ln\left(\frac{V_{C\,max}}{V_C} - 0.999\right)$	if $\frac{V_C}{V_{C\,max}} \geq 0.5$
	$= 0$	if $\frac{V_C}{V_{C\,max}} \leq V_{C\,crit}$
Upper airways resistance	$R_u = A_u + K_u \lvert \dot{V}_{CW} \rvert$	
Collapsible airways resistance	$R_c = K_c (V_{C\,max}/V_C)^2$	
Small airways resistance	$R_s = A_s\, e^{K_s \cdot (V_A - RV)/(V^* - RV)} + B_s$	

*Pleural pressure, P_{pl}, measurements are used to determine P_{mus} when comparing model generated data with experimental data.

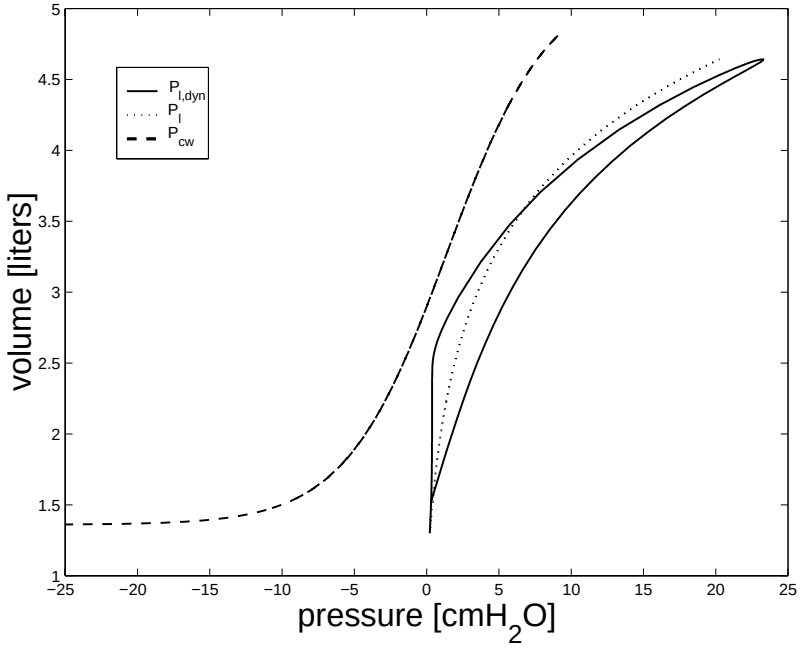

Fig. 2. Chest wall and lung tissue characterizations for subject 1. The maneuver shown corresponds to a simulated vital capacity effort (11.6 s duration). P_{cw}: chest wall elastic recoil; $P_{l,dyn}$: dynamic lung elastic recoil; P_l: static lung elastic recoil.

range of quiet breathing and saturating at higher and lower volumes. We mimic this relationship with a logarithmic expression,

$$P_{cw} = A_{cw} - B_{cw} ln \left(\frac{TLC - RV}{V_{CW} - RV} - 0.999 \right) , \tag{2}$$

where A_{cw}, B_{cw} are constants, TLC is the total lung capacity of each subject and RV the residual volume. Numerical values appearing in Eq. (2) are chosen so that chest wall compliance, $C_{cw} = dP_{cw}/dV_{CW}$, is approximately 0.2 l/cmH_2O in the linear range (volumes of 2.5 to 3 liters), for the subject tested. During tidal breathing the chest wall has mostly an outward recoil, as shown in Fig. 2.

Table 3. Model parameters for volunteer subjects.

Parameter	Units	Subject 1	Subject 2	Subject 3	Subject 4
A_c	cmH_2O	7.09	8.27	9.39	10.67
A_{cw}	cmH_2O	1.4	1.4	1.4	4.4
A_l	cmH_2O	0.2	0.04	0.1	0.57
A_s	cm$H_2O \cdot l^{-1} \cdot s^{-1}$	2.2	2.8	2.47	5.47
A_u	cm$H_2O \cdot l^{-1} \cdot s^{-1}$	0.34	0.31	0.31	0.31
B_c	cmH_2O	37.3	66.8	94.9	127.0
B'_c	cmH_2O	3.73	6.69	9.50	12.7
B_{cw}	cmH_2O	−3.5	−3.5	−3.5	−3.5
B_l	cmH_2O	−0.5	1.0	1.5	0.0
B_s	cm$H_2O \cdot l^{-1} \cdot s^{-1}$	0.02	0.02	0.02	0.02
C_{ve}	l/cmH_2O	0.5	0.5	0.5	0.5
K_c	cm$H_2O \cdot l^{-1} \cdot s^{-1}$	0.21	0.49	0.50	0.24
K_l		1.0	1.0	1.0	0.8
K_s		−10.9	−9.9	−6.5	−5.13
K_u	cm$H_2O \cdot l^{-2} \cdot s^{-2}$	0.46	0.40	0.32	0.20
R_{ve}	cm$H_2O \cdot l^{-1} \cdot s$	1.0	1.0	1.0	1.0
V^*	liters	5.3	10.3	8.41	7.37
$V_{C_{max}}$	liters	0.185	0.125	0.165	0.101

2.2.2. *Lung Tissue*

The viscoelastic behavior of lung tissue has been identified experimentally and it is reported in the literature [30]. In order to capture this behavior, we have replaced the P-V characterization of lung tissue appearing in [15], with the viscoelastic unit shown in Fig. 1B.

Linear viscoelastic structures (Kelvin bodies) have been shown to successfully simulate lung tissue behavior for small volume excursions, including the dependence of tissue compliance and resistance upon the frequency of breathing [14,31]. A nonlinear variation of the Kelvin body is employed here, that accounts, in addition, for the dependence of static tissue compliance upon large volume excursions (static compliance is lower at higher volumes).

The corresponding structure of Fig. 1B employs a combination of a nonlinear compliance C_l in series with a linear spring C_{ve} and resistance R_{ve}. The total pressure drop across these elements is the dynamic elastic recoil of lung tissue, $P_{l,dyn}$, comprising both the elastic and viscous forces. It is expressed as

$$P_{l,dyn} = P_l + R_{ve}(\dot{V}_A - \dot{V}_{VE}) \tag{3}$$

$$= P_l + \frac{1}{C_{ve}} V_{VE}\,, \tag{4}$$

where P_l is the pressure across the static, nonlinear compliance C_l, V_A is the lung volume (volume of compliance C_l), and V_{VE} is the volume of compliance C_{ve}. Coefficients R_{ve} and C_{ve} have constant values chosen to match experimental records of volume and flow.

$P_{l,dyn}$ is plotted in Fig. 2 against V_A. The curve exhibits hysteresis due to the action of nonelastic forces developed in the tissue (resistance R_{ve}). P_l is chosen to bear a nonlinear dependence upon V_A, as shown in Fig. 2, and according to the formula,

$$P_l = A_l \cdot e^{K_l \cdot V_A} + B_l\,. \tag{5}$$

A_l, B_l and K_l are constants chosen so that P_l approximately matches the corresponding static P-V characteristic introduced in [15]. The relationship is almost linear in the quiet breathing range. At higher volumes static compliance decreases.

2.2.3. *Airways*

Functional relationships and parameter values modeling the airways are adopted directly from Liu *et al.* [15], except for the resistive characterization of the peripheral airways which now bear a nonlinear relationship with volume only:

$$R_s = A_s \cdot e^{K_s(V_A - RV)/(V^* - RV)} + B_s\,, \tag{6}$$

where A_s, B_s, K_s and V^* are constants. The corresponding characterization of [15] incorporated an effort dependent term, aimed to achieve the limitation of flow during the expiratory portion of the forced vital capacity maneuver. We replace that mechanism by restricting the airways elastic recoil P_c to positive values only: the airways can now sustain distension, but not compression (see Table 2).

According to Eq. (6), the value of R_s increases exponentially as lung volume V_A decreases. The formula aims to capture the dependence of small airway resistance on lung volume. As the lung inflates, small airways inmbedded into the lung parenchyma are streched open, allowing free passage of airflow (low resistance). At low lung volumes, these airways are constricted, offering large resistance to flow. The value of R_c is inversely proportional to the square of the volume in the airways, V_C (see Table 2). The same principle applies here: as the airways become narrower (lower volume) they offer higher resistance to flow, and vice versa. The characterization of R_c was originally developed in [10] and [23].

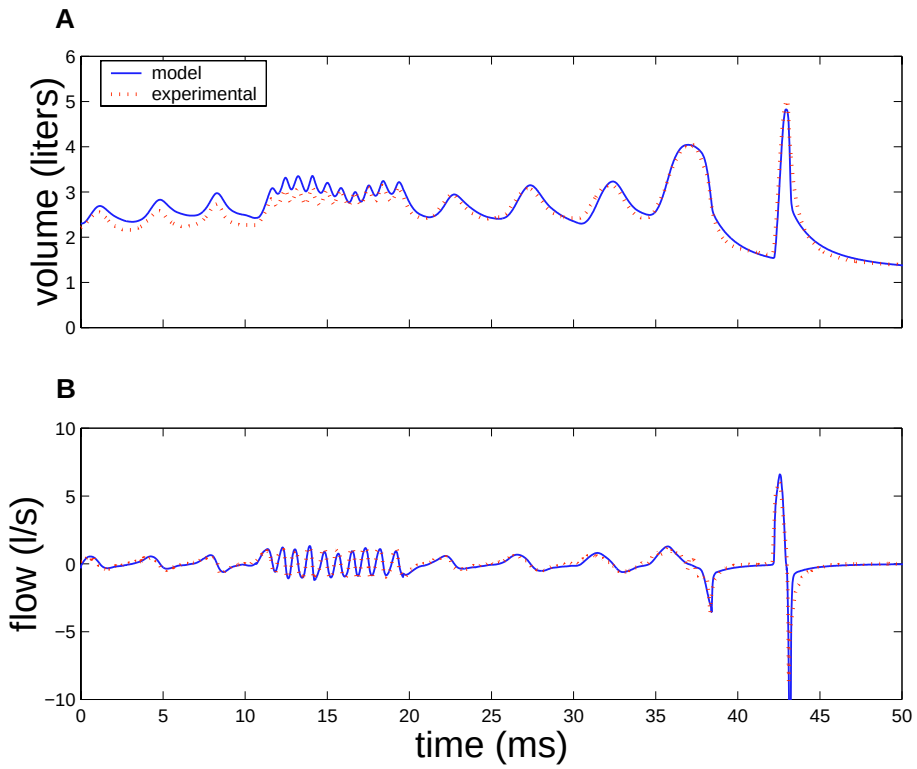

Fig. 3. Experimetal volume (A) and flow (B) waveforms (dotted lines) during spontaneous breathing performed by subject 1 are compared to model predictions (solid lines).

2.2.4. *Full Model of Respiratory Mechanics*

The equations governing the motion of the full model are derived in the Appendix. They are:

$$\begin{bmatrix} R_u + R_c & R_u + R_c & 0 \\ R_u + R_c & R_u + R_c + R_s + R_{ve} & -R_{ve} \\ 0 & -R_{ve} & R_{ve} \end{bmatrix} \begin{bmatrix} \dot{V}_C \\ \dot{V}_A \\ \dot{V}_{VE} \end{bmatrix} + \begin{bmatrix} P_c + P_{cw} \\ P_l + P_{cw} \\ P_{ve} \end{bmatrix} = \begin{bmatrix} P_{mus} \\ P_{mus} \\ 0 \end{bmatrix} . \quad (7)$$

They are solved numerically for the lung volume V_A, the collapsible airways volume V_C and the viscoelastic volume V_{VE}. Figure 3 illustrates the ability of the model to closely match experimental records of volume and flow in three different patterns of breathing performed by a healthy human subject.

2.3. *Work of Breathing*

An analytical expression for the work of breathing is derived in the Appendix [Eq. (A.8)]. The corresponding differential expression for work involves three terms,

each corresponding to one of the independent compliant elements in the model:

$$\begin{aligned} dW = & [P_c + P_{cw} + (R_u + R_c)(\dot{V}_C + \dot{V}_A)]dV_C \\ & + [P_l + P_{cw} + (R_u + R_c)(\dot{V}_C + \dot{V}_A) + R_s\dot{V}_A + R_{ve}(\dot{V}_A - \dot{V}_{VE})]dV_A \\ & + \left[\frac{1}{C_{ve}}V_{VE} + R_{VE}(\dot{V}_{VE} - \dot{V}_A)\right] dV_{VE}\,. \end{aligned} \tag{8}$$

The total work W is computed via numerical integration of the expressions in the brackets over the volume excursion in each compartment and for each breathing maneuver. First, the equations governing the motion of the system (Eqs. (A.7) in the Appendix) are solved. Equation (8) is then evaluated for the model predicted state vector.

The term corresponding to dV_{VE} is identically zero since $\frac{1}{C_{ve}}V_{VE} = -R_{ve}(\dot{V}_{VE} - \dot{V}_A)$ (see Fig. 1B and Fig. 11 in the Appendix). This implies that the energy stored in compliance C_{ve} equals at all times the energy dissipated at resistance R_{ve}. The contribution of the viscoelastic element to the *total* energy of the system is only through the term $R_{ve}(\dot{V}_A - \dot{V}_{VE})$ multiplying dV_A. The term is required, however, in evaluating the elastic (W_{EL}) and dissipative (W_{DIS}) components of work separately. Based on the above formula, it is easy to identify these as:

$$dW_{EL} = (P_c + P_{cw})dV_C + (P_l + P_{cw})dV_A + \frac{1}{C_{ve}}V_{VE}\,dV_{VE} \tag{9}$$

$$\begin{aligned} dW_{DIS} = & (R_u + R_c)(\dot{V}_C + \dot{V}_A)dV_C \\ & + [(R_u + R_c)(\dot{V}_C + \dot{V}_A) + R_s\dot{V}_A + R_{ve}(\dot{V}_A - \dot{V}_{VE})]dV_A \\ & + R_{ve}(\dot{V}_{VE} - \dot{V}_A)dV_{VE}. \end{aligned} \tag{10}$$

Notice that dW_{DIS} includes both flow-resistive and viscoelastic components. The work expended against viscoelastic forces in the lung tissue is:

$$dW_{VE} = R_{ve}(\dot{V}_A - \dot{V}_{VE})dV_A + R_{ve}(\dot{V}_{VE} - \dot{V}_A)dV_{VE}\,. \tag{11}$$

It is of interest to examine the model predicted distribution of dissipative work among the airway resistances. Using Eq. (8) it is easy to write formulas corresponding to work dissipated at resistances R_u, R_c and R_s,

$$dW_{R_u} = R_u(\dot{V}_C + \dot{V}_A)(dV_C + dV_A) \tag{12}$$

$$dW_{R_c} = R_c(\dot{V}_C + \dot{V}_A)(dV_C + dV_A) \tag{13}$$

$$dW_{R_s} = R_s\dot{V}_A\,dV_A\,. \tag{14}$$

Using the analytical expressions developed above, namely Eq. (8) through (14), we predict total work and its components in human subjects (next section) . Given the functional relevance and detail of the model, these predictions will allow a better insight into the energetics of the respiratory system. In particular, they will

identify the work contribution of individual resistances in the airways, and indicate how energy is stored or expended in different types of maneuvers. Emphasis will be given on predictions revealing the role of lung tissue viscoelasticity, especially in maneuvers of increasing frequency.

2.4. *Computational Aspects*

The integrating routine for Eq. (7) is a Runge-Kutta algorithm with adaptive step-size control [27], implemented in the C programming language. The input to the model is measured pleural pressure waveforms, used to compute muscle pressure through Eq. (1). Pleural pressure singals were digitally filtered to remove cardiac artifact. All signals were processed in LabVIEW® software (National Instruments), specifically designed for the experiment [22]. Data were originally processed by Liu *et al.* [15].

3. Results

3.1. *Simulated Work*

A breathing maneuver is simulated at a frequency f of 12 breaths/min and mean total ventilatory rate (frequency $\times$ tidal volume) of 7.2 l/min. We construct the areas dictated by Eq. (8) in the pressure-volume diagram of Fig. 4. Initially, the dynamic recoil of lung tissue, $P_{l,dyn}$, and the static recoil of the chest wall, P_{cw}, are plotted against alveolar volume V_A (ordinate). In this diagram, time progresses in a clockwise sense around the loop, as indicated by the arrows. It should be pointed out that $P_{l,dyn}$, a positive pressure, is mirrored to the left half of the plane according to a scheme introduced by Campbell [8] ([29] provides a detailed description of the Campbell diagram). The area between the two pressure curves ($P_{l,dyn}$ and P_{cw}) equals the elastic work of breathing, W_{EL}, plus the work dissipated in nonelastic tissue, W_{VE} (terms corresponding to dV_A only). The latter equals the area inside the loop formed by $P_{l,dyn}$. The area enclosed by P_{cw} and the line connecting the extrema of the loop (not drawn) equals the purely elastic work.

The areas discussed thus far account for all terms in Eq. (8) (term corresponding to dV_A), except for those involving airway resistances. An additional pressure, namely $(R_u + R_c)(\dot{V}_C + \dot{V}_A) + R_s\dot{V}_A + R_{ve}(\dot{V}_A - \dot{V}_{VE})$ is now superimposed on the diagram. This pressure is equal to the pleural pressure, P_{pl}, and forms a second loop that encloses the hysteresis of lung tissue ($P_{l,dyn}$). The area inside it equals the dissipative work, W_{DIS}.

3.2. *Comparison with Data*

Total work equals the area subtended by the pleural pressure curve and chest wall compliance, as shown in the Campbell diagrams of Fig. 5. Model-predicted volume-pressure relationships are plotted in the same figure and show good agreement. Total work rates and components of work are listed in Table 4.

Table 4. Measured and model predicted work rates.

Maneuver	f, b/min	V_T, liters	$\dot{V}$, l/min	$\dot{W}_{meas}$, J/min	$\dot{W}$, J/min	$\dot{W}_{EL}$, J/min	insp $\dot{W}_{DIS}$, J/min	exp $\dot{W}_{DIS}$, J/min	$\dot{W}_{VE}$, J/min
					subject 1				
Tidal	15	0.50	7.5	3.5	3.16	1.45	0.87	0.61	0.24
Pant	77	0.33	25.4	15.8	13.0	6.44	3.56	3.15	0.14
FVC	5.18	3.6	18.6	181	184	12.3	37.4	145	3.70
					subject 2				
FVC	7.23	7.11	51.4	500	543	28.0	167	370	16.2
					subject 3				
FVC	9.83	4.1	40.3	523	459	17.3	86.3	370	7.57
					subject 4				
FVC	6.42	5.67	36.4	383	397	53.7	101	295	13.9

f, frequency of breathing; V_T, tidal volume; $\dot{V}$, average ventilatory rate ($f \times V_T$); $\dot{W}_{meas}$, measured work rate (assuming chest wall compliance given by Eq. (2)); Model predicted work rates: $\dot{W}$, total; $\dot{W}_{EL}$, elastic; $\dot{W}_{DISS}$, dissipative; $\dot{W}_{VE}$, viscoelastic.

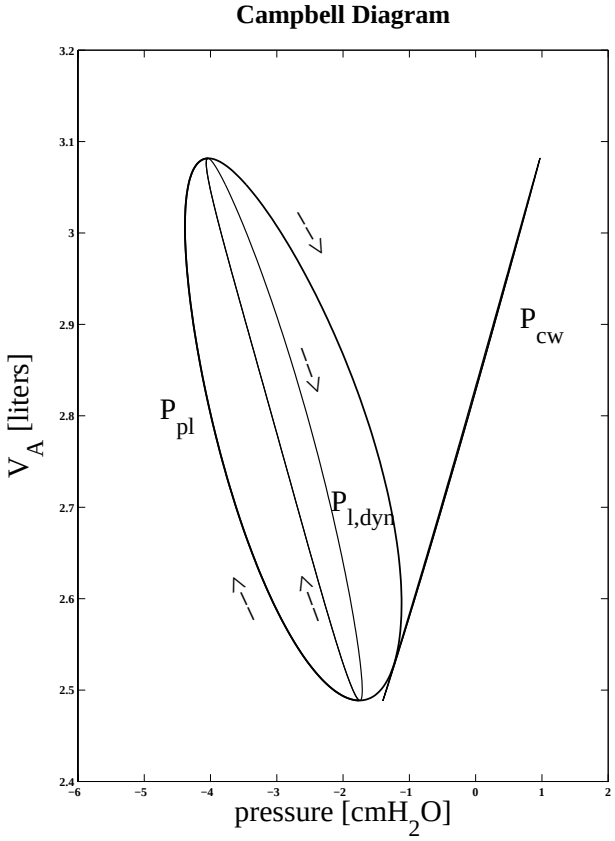

Fig. 4. Pressure-volume diagram depicting work of breathing and its components for a simulated maneuver (see text for explanation).

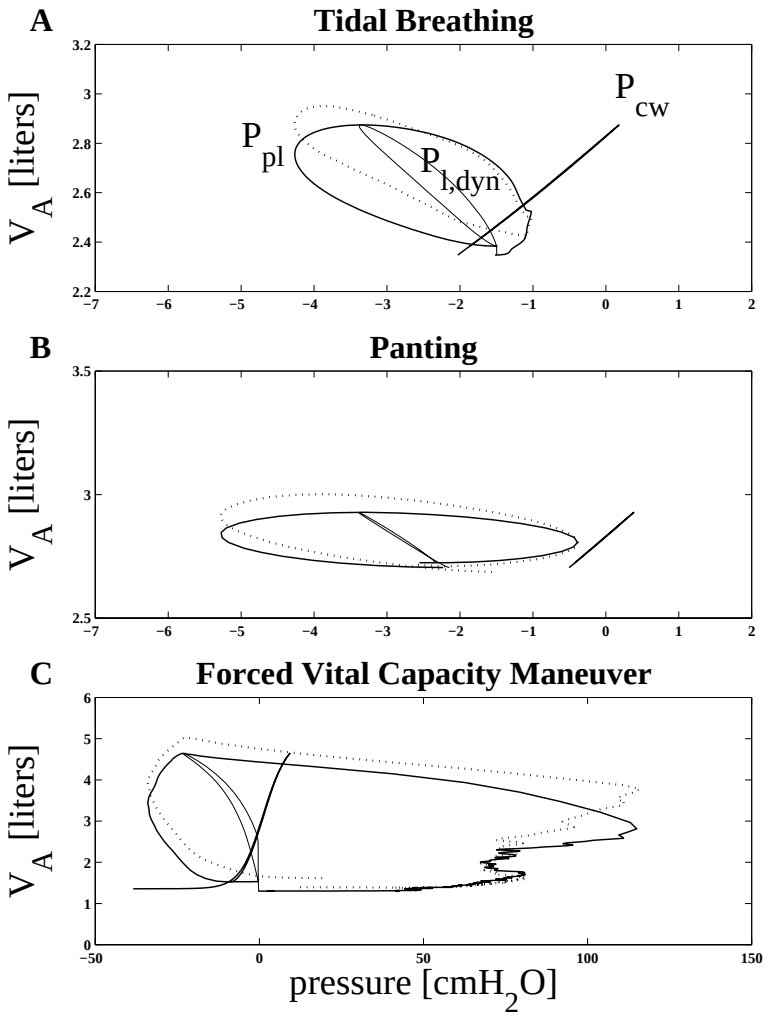

Fig. 5. Campbell diagrams for measured data (dotted lines) and model-generated data (solid lines). A: tidal breathing, B: panting, C: FVC. Dotted loops correspond to pleural pressure and volume measurements. See text for discussion of the relevant areas.

During tidal breathing (Fig. 5A) a work rate of 3.5 J/min is measured, corresponding to a model predicted value of 3.16 J/min. During the inspiratory phase, the muscles of respiration produce work against both the elastic and the dissipative forces in the system (1.45 J/min and 0.87 J/min, respectively). During expiration, energy stored in elastic tissue is released (1.45 J/min, same as for inspiration). Part of it is expended in overcoming the work of resistive forces (0.61 J/min). The remaining released elastic energy (0.84 J/min) is counteracted by persistent contraction of the respiratory muscles. It is therefore the work done by the elastic tissues on the muscles. Equivalently, the muscles do negative work, opposing the return of the system to its equilibrium. The total work (positive plus negative)

done by the muscles is $1.45 + 0.87 + 0.84 = 3.16$ J/min ([29] quotes a nominal value of 4 J/min during "quiet breathing through the nose").

The panting maneuver (Fig. 5B) involves higher rates due to the increased flow (15.8 J/min measured, 13.0 J/min predicted). Also, dissipative work is more equally divided among the inspiratory and expiratory phases. It is unusual that the elastic energy released at expiration (6.44 J/min) is greater than the nonelastic work (3.15 J/min). This implies that negative work must be performed by the muscles in order to account for the surplus in elastic energy. Panting maneuvers usually involve positive expiratory work, indicated by the pleural pressure loop extending to the right of the chest wall compliance, as shown in Fig. 5C for FVC. The FVC maneuver clearly requires a large effort (184 J/min), mostly in overcoming the dissipative work during the expiratory portion of the cycle (145 J/min).

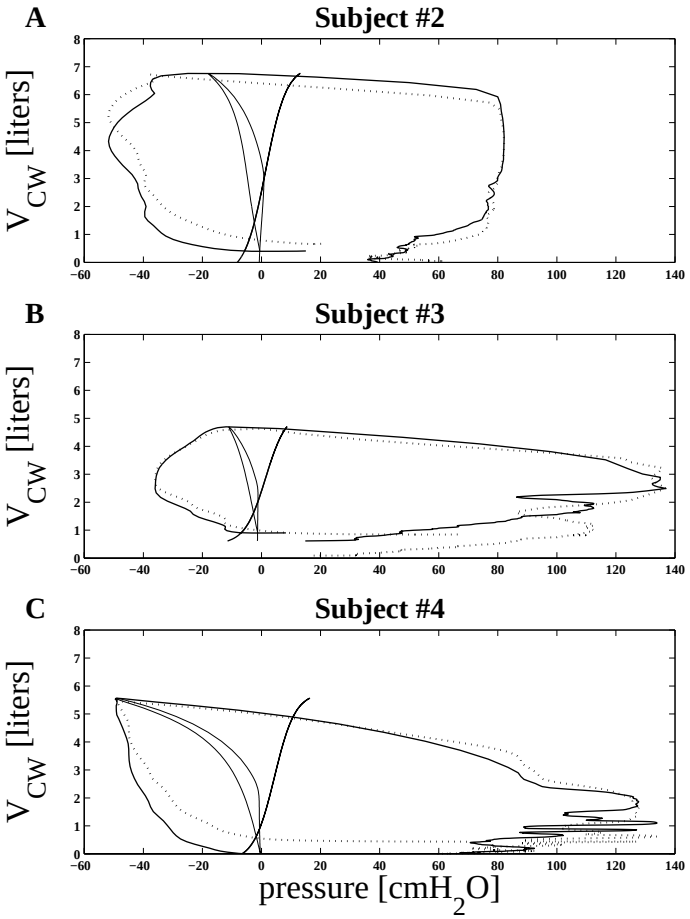

Fig. 6. Campbell diagrams constructed from pleural pressure and volume measurements (dotted lines), and from model-generated data (solid lines), for subjects 2, 3 and 4. See text for discussion of the relevant areas.

Pleural pressure and volume data were collected in the laboratory for three additional healthy subjects. Figure 6 shows Campbell diagrams constructed using the experimental data collected from the FVC maneuver. Model predictions are superimposed and show good agreement, despite the variability in the data. The nominal parameter set changes for each subject, as shown in Table 3. Total work rates for the FVC maneuver, listed in Table 4, range from 184 J/min (subject 1) to 543 J/min (subject 2), corresponding to measured values of 181 J/min and 500 J/min, respectively. Elastic work is a small fraction of the total work and it is recovered almost entirely during expiration (i.e., no negative work is required to overcome the released elastic energy during expiration). This is evident in both the pressure-volume diagrams of Fig. 6 (pleural pressure loop encloses all areas) and in Table 4, where total dissipative work (inspiratory and expiratory) is approximately equal to the total work of breathing. Dissipative work during expiration is 2.2 to 3.9 times greater than that during inspiration. In the FVC maneuver, the flow is maximum shortly after expiration commences. Dissipative work is proportional to flow, as suggested by Eq. (10), and thus assumes a great value during expiration. Moreover, the FVC effort involves a prolonged expiratory effort (as clearly depicted in Fig. 8, third column), which also results in the accumulation of dissipated energy. Viscoelastic work is only about 1.7–3.0% of the total energy dissipated.

3.3. *Distribution of Dissipative Work*

Figure 7 shows pressure-volume diagrams that correspond to the volume integrals of Eqs. (12), (13) and (14), for the three spontaneous breathing patterns performed by subject 1. Time follows a counterclockwise direction along the loops (unlike the pleural pressure loops), and inspiration corresponds to the right half plane (where flow is positive). Quiet breathing expends more energy during the inspiratory phase of the cycle, in all three resistances. The resistance of the collapsible airways dissipates the greatest amount of energy. During panting, dissipated work is equally divided among inspiration and expiration. Resistive work at the upper and collapsible airways dominates during the forced vital capacity maneuver, especially at the expiratory phase. W_{R_u} exhibits a peak at the beginning of expiration, when the flow is maximum (recall that R_u is flow dependent). W_{R_c} peaks towards the end of expiration, as the airways collapse and the value of R_c increases. Work done against resistive forces at the small airways dominates at the beginning of inspiration: the large initial flow of the maneuver, combined with a high R_s value (the maneuver is initiated at RV) yield the observed effect.

An alternative presentation of the same results gives additional insight into the distribution of energy. Figure 8 plots dissipative work components in a power vs. time format. The dynamic distribution of work, represented by the filled areas, and the delineation of breathing phases, are more evident here. During tidal breathing, for instance, it is clear that the increased dissipation in the inspiratory phase is due to a higher peak in the power. Expiratory power peaks at lower levels and

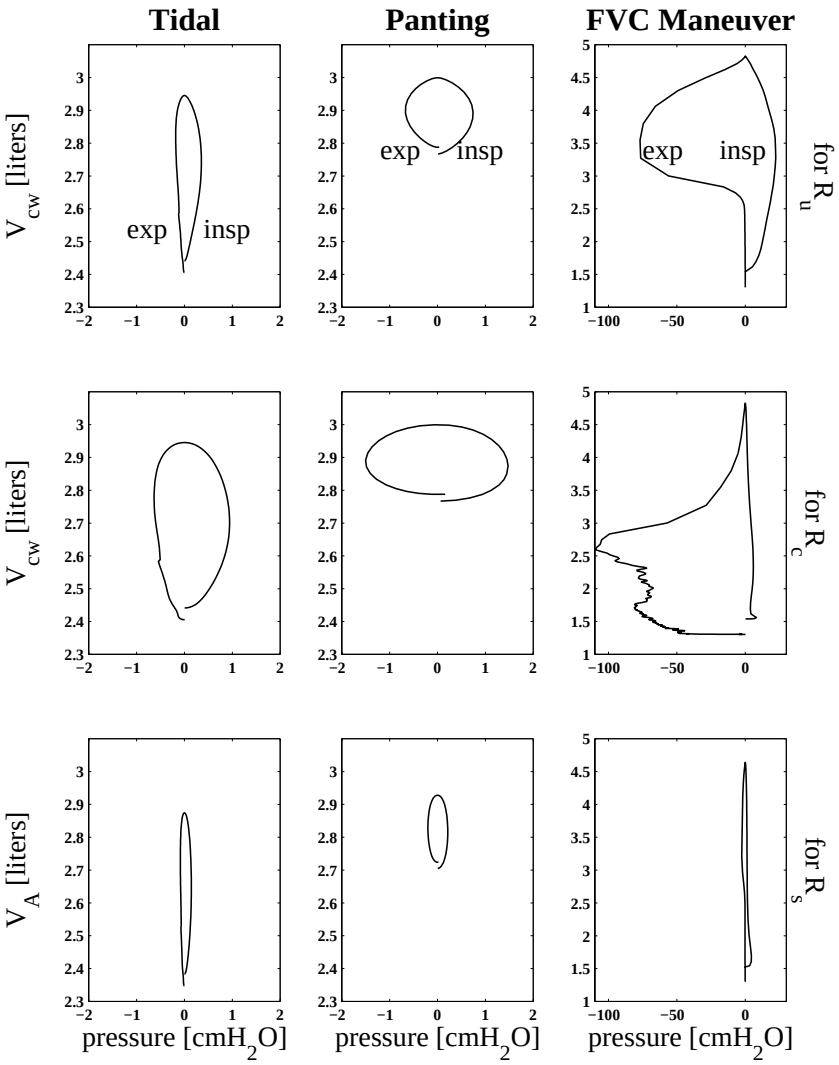

Fig. 7. Model predicted distribution of dissipative work among airway resistances.

lasts longer. On the other hand, panting exhibits a clear symmetry in power. The FVC maneuver involves sharp peaks concentrated at the beginning of expiration; dissipation at the collapsible resistance is the only one persisting throughout the cycle.

3.4. *Effect of Frequency*

Table 5 lists model predicted average work rates $\dot{W}$ corresponding to simulated maneuvers at frequencies ranging from 3 to 60 breaths/min. Average alveolar ventilation $f \cdot V_A^*$, where V_A^* is the portion of V_{CW} that contributes to alveolar ventilation

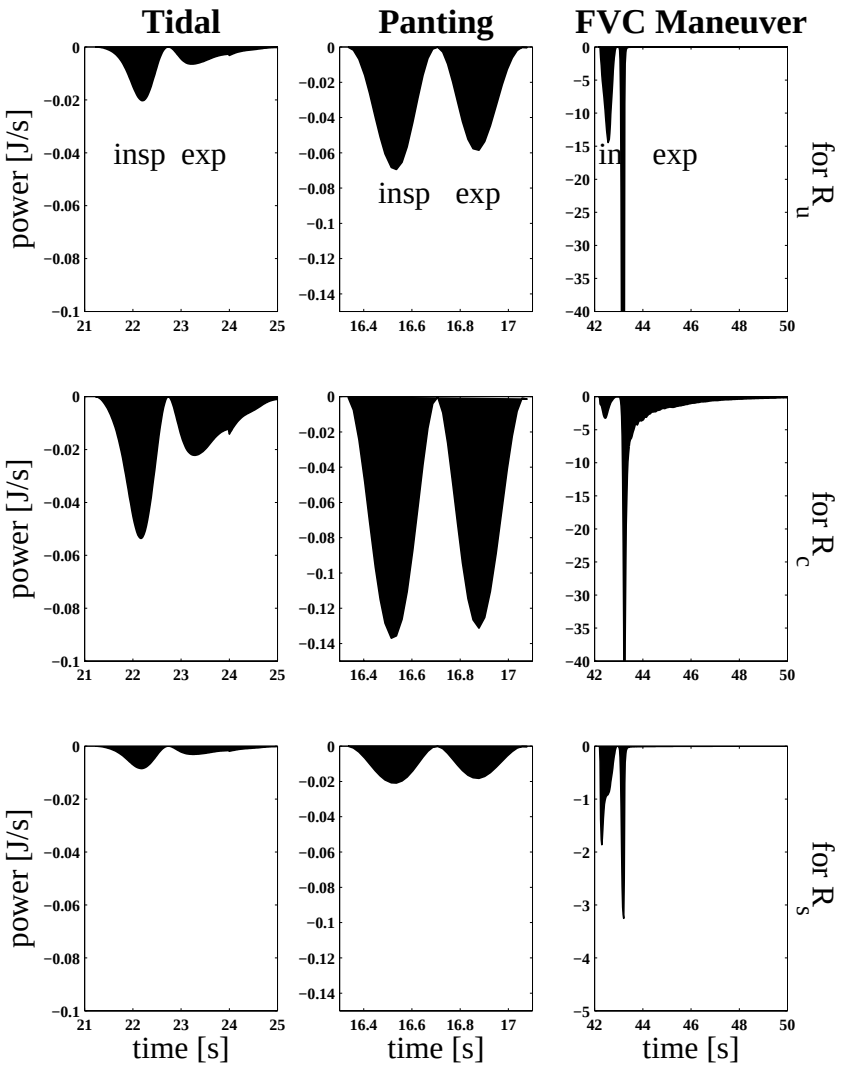

Fig. 8. Model predicted distribution of dissipative work among airway resistances in a power vs. time format.

($V_A^* = V_{CW} - V_D$), is kept constant at 6.0 l/min (V_D is the volume of the dead-space). The input function P_{mus} is adjusted to generate volumes V_{CW} that satisfy the above relations, or, equivalently, $V_{CW} = (6.0 + f\,V_D)/f$. Total ventilation $\dot{V}_E$ increases as frequency increases according to the relation, $\dot{V}_E = f\,V_{CW} = fV_A^* + fV_D$.

Figure 9 shows that according to model predictions work rate exhibits a minimum at a frequency around 10 breaths/min and its value increases both at higher and lower frequency maneuvers. Elastic work decreases initially, reaching a minimum at around 20 breaths/min, yet it climbs up again for maneuvers at higher frequencies. This is attributed to the stiffening of lung tissue with increasing

Table 5. Effect of increasing frequency on work.

f, breaths/min	A_{mus}, cmH_2O	V_T, liters	$\dot{W}$, J/min	$\dot{W}_{EL}$, J/min	$\dot{W}_{DIS}$, J/min
3	14.0	2.2	7.62	7.09	0.53
5	6.30	1.4	4.62	4.01	0.61
8	4.00	0.95	3.68	2.94	0.74
12	3.10	0.70	3.53	2.62	0.91
20	2.50	0.50	3.66	2.50	1.16
30	2.40	0.40	4.52	2.91	1.61
45	2.45	0.33	5.94	3.65	2.29
60	2.50	0.30	6.78	4.05	2.73

Average alveolar ventilation was kept constant at 6 liters/min for all maneuvers. Simulations were generated with a sinusoidal muscle pressure of the form $P_{mus} = A_{mus} \cdot sin(2\pi ft) + A_{mus}$, where A_{mus} is given in the table and t is time. f, frequency of breathing; V_T, tidal volume; Model predicted work rates: $\dot{W}$, total; $\dot{W}_{EL}$, elastic; $\dot{W}_{DIS}$, dissipative.

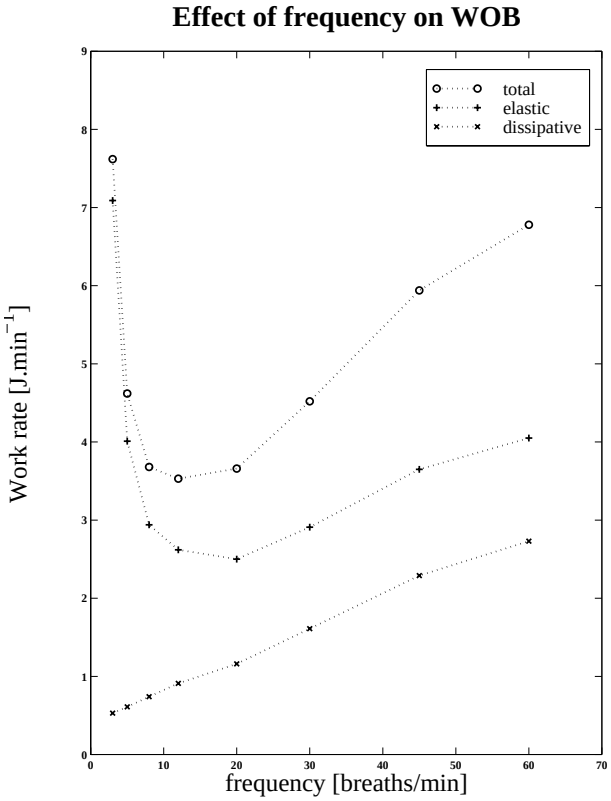

Fig. 9. Effect of frequency of breathing upon model-generated WOB at a constant alveolar level. Simulated maneuvers correspond to those listed in Table 5.

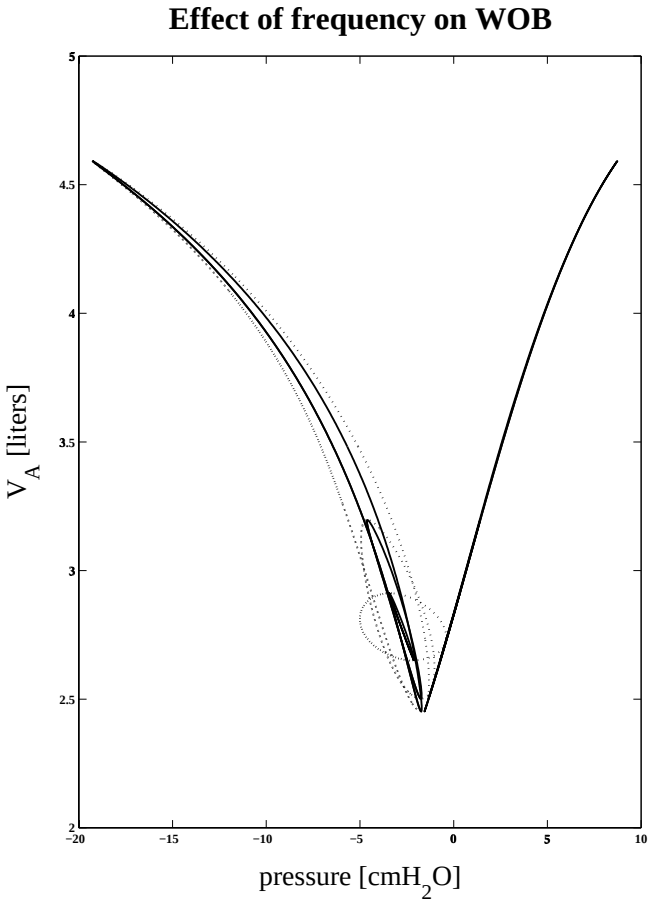

Fig. 10. Campbell diagram identifying work of breathing at frequencies of 3 (tall loop), 12 (middle loop) and 60 breaths/min (short loop), at constant alveolar ventilation. Pleural pressure loops (dotted lines) become wider with increasing frequency, signifying the increase in dissipated work. Dynamic lung compliance decreases resulting in increased elastic energy.

frequency. Figure 10 illustrates this effect in a Campbell diagram for the lung compartment that superimposes the simulated maneuvers of Table 5. The static compliance of the chest wall remains the same, while the dynamic compliance of lung tissue decreases with increasing frequency (slope of solid line loops has tilted to the left). Pleural pressure loops (dotted lines) become wider, signifying an increase in the flow-resistive work, attributed to the extra flow required to sustain a high frequency maneuver.

4. Discussion

4.1. *Work of Breathing*

Clinical accounting of WOB involves a single independent volume variable (the

equivalent of the volume in the chest wall compartment $V_{CW} = V_A + V_C$ in this model), that characterizes the compliance of the total respiratory system. Airways are assumed rigid and a single resistance is usually employed to characterize them. In contrast, our analysis identifies formulas that predict work of breathing (WOB) and its components using a nonlinear model of the respiratory system. The model incorporates three airway resistances, a collapsible airways compartment, a lung tissue characterization including viscoelastic properties, and a chest wall characterization.

During quiet breathing, dissipative work accounts for 37.5% of inspiratory work (subject 1). This percentage remains roughly the same during panting, but increases to twice that value for the FVC maneuver. Elastic energy released during expiration overcompensates for all resistive and viscoelastic losses during tidal breathing and panting, to the extent that negative work is required by the muscles. Its net effect on the FVC maneuver is negligible because dissipation is greater than the released elastic energy. In tidal breathing, work done against viscoelastic forces is 16.2% of the total dissipation (inspiration plus expiration). This percentage drops to a value ranging from 1.67% to 3.5% for both the FVC and panting (all subjects).

4.2. *Forced Vital Capacity Maneuver*

We have shown that elastic work, W_{EL}, during the FVC maneuver is a small portion of the total work of breathing (see Table 4). Most work is expended to overcome the dissipative forces, especially in the expiratory phase of the cycle. Elastic work reflects potential energy and is, therefore, a function of volume excursion only (for a constant frequency of breathing): the deeper the maneuver, the more energy stored upon inspiration and the more energy released upon expiration. Dissipative work, W_{DIS}, on the other hand, involves non-conservative forces and thus depends upon the path traveled. Forceful efforts, such as the FVC, require large pressures (see pleural pressure path in Fig. 6), which in turn result in a large W_{DIS}. Since the elastic work remains the same, it appears as a smaller portion of the total work. If the same maneuver were conducted without a forceful effort, W_{EL} would be a higher portion of the total work (as it is for quiet breathing). For instance, following a full expiration, a relaxed expiration is passive (up to the functional residual capacity), meaning that released stored energy compensates for the dissipative forces. Flow-limited patients have to breathe forcefully, thus generating larger W_{DIS}, whereas their elastic work remains the same (for maneuvers of the same volume excursion and frequency of breathing).

4.3. *Distribution of Dissipated Work*

We further identify the contribution on WOB of respiratory components that are difficult or even impossible to measure. Figure 7 illustrates the distribution of flow-resistive work among three different types of resistances in the airways. The model predicts that at the beginning of expiration energy losses in the upper airways dom-

inate; the collapsible airways dissipate most energy at the latter part of expiration. Work expended against the small airways peaks at the beginning of inspiration.

4.4. *Frequency Dependence*

Model predictions show that increasing the frequency of breathing while maintaining a constant ventilatory rate affects WOB in the following manner (Fig. 9): i) elastic work initially drops to a minimum around 20 breaths/min and ramps up again at higher frequencies; ii) dissipative work increases continuously; and iii) as a result total work exhibits a minimum around 12 breaths/min. This is in good agreement with experimental results suggesting that at a given ventilatory level, an optimal frequency exists for which the work of breathing is minimized. While Rohrer [28] first suggested this in 1925, it was verified in experiments for human and animal subjects two decades later [9,18,20]. In addition, Otis *et al.* [26] have described the relationship mathematically in a simple one-compartment, capacitative model of respiratory mechanics. They indicated that while flow-resistive work increases with increasing frequency, elastic work drops to a constant level (due to decreasing volume). As a result, the sum of the two, comprising the total work, assumes a minimum at a certain frequency. Our results show that elastic work increases at higher frequencies due to the reduced compliance of lung tissue, as depicted in Fig. 10. This observation is in agreement with published experimental results on lung tissue, the compliance of which has been shown to decrease with increasing frequency.

4.5. *Model Limitations*

1. The viscoelastic behavior of the chest wall has not been modeled. Most researchers address lung tissue viscoelasticity but not chest wall viscoelasticity, as the latter is probably less significant (in terms of hysteresis in the P-V loop and, therefore, lost work). Sharp *et al.* [30] have confirmed this experimentally in healthy anesthetized human subjects. This is also reflected in the measurement of WOB, whereby both elastic and dissipative energy in the chest wall are neglected (WOB is commonly approximated by the area enclosed inside the pleural pressure loop).

2. Work measured with the esophageal balloon technique does not account for the dissipative forces developed in the chest wall tissue. In addition, work done against the elastic forces of the total respiratory system (both lung and thorax) can be identified only if the static compliance of the thorax is measured, as well. As mentioned earlier, we have not collected measurements on chest wall behavior.

3. The modeling effort presented here only addresses normal respiratory system operation. We have not investigated the effect of disease on WOB, although the model has the ability to simulate altered mechanical behavior in the system, as demonstrated in [15], where we conducted an extensive sensitivity analysis of the original model.

Limitations like the ones discussed here are common in every modeling effort. The proposed model is detailed enough to capture the nonlinear dynamic behavior of the respiratory system, and, at the same time, simple enough to allow experimental validation using noninvasive procedures.

4.6. *Summary*

Using a nonlinear model of respiratory mechanics we have i) predicted total WOB values in spontaneous breathing maneuvers that compare well with experimental data; ii) identified the contribution of three different types of resistances in the airways; iii) simulated the behavior of the respiratory system to minimize WOB by selecting an optimal frequency at a given ventilatory rate; and iv) identified the role of lung tissue viscoelasticity in achieving that behavior.

Our results show that the proposed model can successfully mimic complex respiratory dynamics, such as frequency dependent and nonlinear behavior (validation), and, at the same time, identify the dynamic behavior of elements the contribution of which to the work of breathing cannot be measured noninvasively (prediction). As such, the model lays the framework for investigating the energy pattern of disease in respiratory mechanics. Although abnormalities in respiratory mechanics have not been addressed here, the model can be easily adjusted to account for different pathologies. Experimental validation will be required, however.

The benefit of our analysis lies in the fact that we are able to account for the work associated with breathing in three different maneuvers, more fully and more precisely than what was allowed by conventional models of respiratory mechanics. This ability is afforded by the completeness of the proposed model and its nonlinear nature.

Appendix

The equations governing the motion of the system are developed using a Lagrangian analysis [11,19]. The analysis included here will establish the equations in a form that provides insight into the energy components associated with the model. In particular, the equations are written such that the elastic and dissipative forces and the energy associated with these forces in the system are clearly identified.

The dynamic behavior of the system is described completely by generalized coordinates whose number is equal to the number of energy storage elements minus the number of constraints [11]. In the absence of inertial elements, kinetic energy is zero and potential energy is stored in the four compliant compartments. Due to the kinematic constraint $V_{CW} = V_A + V_C + V_D$, however, only three independent generalized coordinates are realized, namely, $q_1 = V_C$, $q_2 = V_A$ and $q_3 = V_{VE}$, depicted in the mechanical representation of the model in Figure 11 (V_D is the volume of the dead space).

Lagrange's equation [11,19] applicable to each generalized coordinate q_i is then

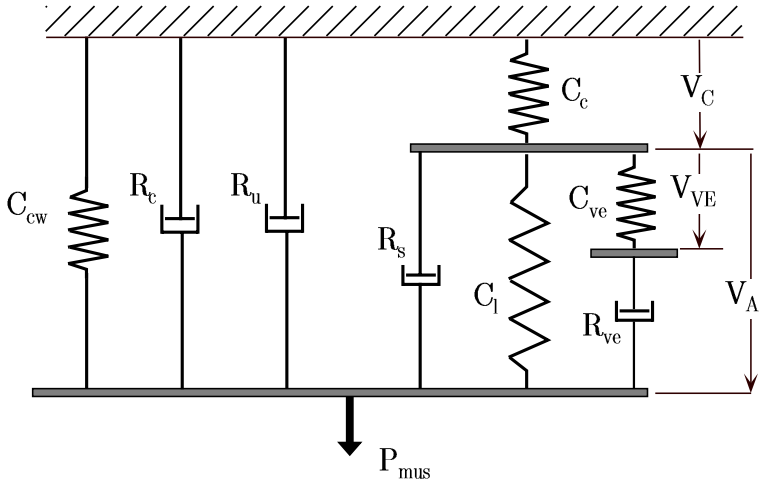

Fig. 11. Mechanical equivalent of respiratory mechanics model.

given as:

$$\frac{\partial E_{pot}}{\partial q_i} = Q_{nc_i} \qquad \text{for} \quad i = 1, 2\,. \tag{A.1}$$

where E_{pot} is the potential energy of the system and Q_{nc_i} the sum of all nonconservative, generalized forces that correspond to the coordinate q_i. They include the externally applied muscle pressure P_{mus} and the pressure drop P_{diss} across resistive elements in Fig. 1B. In the case of viscous damping $P_{diss} = -R\dot{q}$, where R is the resistive coefficient that corresponds to the time derivative of coordinate q (the minus sign indicates that the force acts in a direction opposite to that of the velocity). In the context of Lagrangian dynamics the total virtual work for this system (**not** to be confused with work of breathing) can be easily calculated [11,19] and is given as:

$$\begin{aligned}\delta W = {} & [P_{mus} - (R_u + R_c)(\dot{V}_C + \dot{V}_A)]\ \delta V_C \\ & + [P_{mus} - (R_u + R_c)(\dot{V}_C + \dot{V}_A) - R_s\dot{V}_A - R_{ve}(\dot{V}_A - \dot{V}_{VE})]\ \delta V_A \\ & + [R_{ve}(\dot{V}_A - \dot{V}_{VE})]\delta V_{VE}\,,\end{aligned} \tag{A.2}$$

where δV_C, δV_A and δV_{VE} are virtual displacements. The nonconservative forces for each generalized coordinate are then given by the terms multiplying the corresponding virtual displacement, or:

$$Q_{nc_1} = P_{mus} - (R_u + R_c)(\dot{V}_C + \dot{V}_A) \tag{A.3}$$

$$Q_{nc_2} = P_{mus} - (R_u + R_c)(\dot{V}_C + \dot{V}_A) - R_s\dot{V}_A - R_{ve}(\dot{V}_A - \dot{V}_{VE}) \tag{A.4}$$

$$Q_{nc_3} = R_{ve}(\dot{V}_A - \dot{V}_{VE}). \tag{A.5}$$

Potential energy is given by the general formula, $E_{pot} = -\int_q^{q_{ref}} P\,dq$, where P is the generalized elastic force, in this case the pressure drop across a compliant

element. The integral is evaluated from the current coordinate value q to a reference (fixed) value q_{ref}. The elastic forces that correspond to coordinates V_C, V_A and V_{VE} are pressures $(P_c + P_{cw})$, $(P_l + P_{cw})$ and P_{ve}, respectively. The total potential energy is

$$E_{pot} = \int_0^{V_C} (P_c + P_{cw})\, dV_C + \int_0^{V_A} (P_l + P_{cw})\, dV_A + \int_0^{V_{VE}} P_{ve}\, dV_{VE}. \quad \text{(A.6)}$$

Note that the minus sign of the general equation is canceled by the reversal of the integration limits in Eq. (A.6). Also, due to the conservative nature of the elastic forces, reference positions are arbitrarily set to zero.

The equations of motion can now be obtained by substituting Eqs. (A.3) to (A.6) into Lagrange's formula and rearranging. In matrix form the equations are

$$\begin{bmatrix} R_u + R_c & R_u + R_c & 0 \\ R_u + R_c & R_u + R_c + R_s + R_{ve} & -R_{ve} \\ 0 & -R_{ve} & R_{ve} \end{bmatrix} \begin{bmatrix} \dot{V}_C \\ \dot{V}_A \\ \dot{V}_{VE} \end{bmatrix} + \begin{bmatrix} P_c + P_{cw} \\ P_l + P_{cw} \\ P_{ve} \end{bmatrix} = \begin{bmatrix} P_{mus} \\ P_{mus} \\ 0 \end{bmatrix}. \quad \text{(A.7)}$$

The temporal variation of the generalized coordinates V_C, V_A and V_{VE} is described by three coupled, nonlinear, ordinary differential equations. P_{mus} is the independent, time-varying input function resulting from a particular breathing pattern.

The first term on the left side of Eq. (A.7) represents the dissipative forces introduced by the four resistances in the model while the second term on the left side of the equation represents the elastic forces that characterize the compliant elements. The term on the right side of Eq. (A.7) represents the applied force. The force balance can be transformed into an energy balance by multiplying with a differential displacement and integrating:

$$\begin{aligned} W = & \int_0^{V_C} [P_c + P_{cw} + (R_u + R_c)(\dot{V}_C + \dot{V}_A)] dV_C \\ & + \int_0^{V_A} [P_l + P_{cw} + (R_u + R_c)(\dot{V}_C + \dot{V}_A) + R_s \dot{V}_A + R_{ve}(\dot{V}_A - \dot{V}_{VE})] dV_A \\ & + \int_0^{V_{VE}} [P_{ve} + R_{ve}(\dot{V}_{VE} - \dot{V}_A)] dV_{VE}\,. \end{aligned} \quad \text{(A.8)}$$

References

[1] A. Armaganidis and C. Roussos, Measurement of the work of breathing in the critically ill patient. In *The Thorax*, 2nd Edition, ed. by C. Roussos (Marcel Dekker, New York, 1995).

[2] M. J. Banner, Respiratory muscle function and the work of breathing: Clinical implications, *Crit. Care Updates* **2** (1995) pp. 1–18.

[3] M. J. Banner, M. J. Jaeger and R. R. Kirby, Components of the work of breathing and implications for monitoring ventilator-dependent patients, *Crit. Care Med.* **22** (1994) pp. 515–523.

[4] M. J. Banner, R. R. Kirby and P. B. Blanch, Site of pressure measurement during spontaneous breathing with continuous positive airway pressure: Effect on calculating imposed work of breathing, *Crit. Care Med.* **20** (1992) pp. 528–533.
[5] M. J. Banner, R. R. Kirby, P. B. Blanch and A. J. Layon, Decreasing imposed work of the breathing apparatus to zero using pressure-support ventilation, *Crit. Care Med.* **21** (1993) pp. 1333–1338.
[6] M. J. Banner, R. R. Kirby, A. Gabrielli, P. B. Blanch and A. J. Layon, Partially and totally unloading respiratory muscles based on real-time measurements of work of breathing: A clinical approach, *Chest* **106** (1994) pp. 1835–1842.
[7] P. B. Blanch and M. J. Banner, A new respiratory monitor that enables accurate measurement of work of breathing: a validation study, *Respir. Care* **39** (1994) pp. 897–905.
[8] E. J. M. Campbell, *The Respiratory Muscles and the Mechanics of Breathing* (Year Book Publishers, Chicago, 1958).
[9] M. L. Crosfill and J. G. Widdicombe, Physical characteristics of the chest and lungs and the work of breathing in different mammalian species, *J. Physiol. London* **158** (1961) pp. 1–14.
[10] J. F. Golden, J. W. Clark and P. M. Stevens, Mathematical modeling of pulmonary airway dynamics, *IEEE Trans. Biomed. Eng.* **BME-20** (1973) pp. 397–404.
[11] D. T. Greenwood, *Classical Dynamics*, (Prentice Hall, Englewood Cliffs, 1977).
[12] A. C. Guyton, *Textbook of Medical Physiology*, (W.B. Saunders Company, Philadelphia, 1991), 8th edition.
[13] A. T. Johnson, *Biomechanics and Exercise Physiology* (John Wiley & Sons, New York, 1991).
[14] B. Jonson, L. Beydon, K. Brauer, C. M.ansson, S. Valind and H. Grytzell, Mechanics of respiratory system in healthy anesthetized humans with emphasis on viscoelastic properties, *J. Appl. Physiol.* **75** (1993) pp. 132–140.
[15] C. H. Liu, S. C. Niranjan, J. W. Clark, Jr., K. Y. San, J. B. Zwischenberger and A. Bidani, Airway mechanics, gas exchange, and blood flow in a nonlinear model of the normal human lung, *J. Appl. Physiol.* **84** (1998) pp. 1447–1469.
[16] K. R. Lutchen, F. P. Primiano and G. M. Saidel, A nonlinear model combining pulmonary mechanics and gas concentration dynamics, *IEEE Trans. Biomed Eng.* **BME-29** (1982) pp. 629–641.
[17] J. J. Marini, Work of breathing during mechanical ventilation, *Update on Intensive Care and Emergency Medicine*, ed. by J. L. Vincent (Springer Verlag, 1990), pp. 239–251.
[18] M. R. McIlroy, R. Marshall and R. V. Christie, Work of breathing in normal subjects, *Clin. Sci.* **13** (1954) pp. 127–136.
[19] J. Meisel, *Principles of Electromechanical-Energy Conversion* (McGraw-Hill, New York, 1966).
[20] G. Milic-Emili and J. M. Petit, Il lavoro mechanico della respirazione a varia frequenza respiratoria, *Arch. Sci. Biol. Bologna* **43** (1959) pp. 326–330.
[21] J. Milic-Emili, J. Mead, J. M. Turner and E. M. Glauser, Improved technique for estimating pleural pressure from esophageal balloons, *J. Appl. Physiol.* **19** (1964) pp. 207–211.
[22] J. B. Olansen, F. Ghorbel, J. W. Clark, Jr., D. Deyo, J. B. Zwischenberger and A. Bidani, An automated labview-based data acquisition system for the analysis of pulmonary function, *J. Clin. Engineering* **23** (1998) pp. 279–287.

[23] M. F. Olender, J. W. Clark and P. M. Stevens, Analog computer simulation of maximum expiratory flow limitation, *IEEE Trans. Biomed. Eng.* **BME-23** (1976) pp. 445–452.
[24] A. B. Otis, The work of breathing, *Physiol. Rev.* **34** (1954) pp. 449–458.
[25] A. B. Otis, The work of breathing, in *Handbook of Physiology: A Critical, Comprehensive Presentation of Physiological Knowledge and Concepts*, Sec.3: Respiration, ed. by W. O. Fenn and H. Rahn, (American Physiological Society, Washington, 1964).
[26] A. B. Otis, W. O. Fenn and H. Rahn, Mechanics of breathing in man, *J. Appl. Physiol.* **2** (1950) pp. 592–607.
[27] W. H. Press, S. A. Teukolsky, W. T. Vetterling and B. P. Flannery, *Numerical Recipes in C: The Art of Scientific Computing* (Cambridge University Press, 1992).
[28] F. Rohrer, *Handbuch der normalen und pathologischen Physiologie*, *Physiologie der Atembewegung*, ed. by A. T. J. Bethe, G. von Bergmann, G. Embden and A. Ellinger (Springer Verlag, 1925), pp. 70–127.
[29] C. Roussos and E. J. M. Campbell, Respiratory muscle energetics, *Handbook of Physiology*, Section 3, revised: *The Respiratory System, Volume III* (American Physiological Society, 1987), pp. 481–509.
[30] J. T. Sharp, F. N. Johnson, N. B. Goldberg and P. van Lith, Hysteresis and stress adaptation in the human respiratory system, *J. Appl. Physiol.* **23** (1967) pp. 487–497.
[31] C. Svantesson, J. John, V. Taskar, E. Evander and B. Jonson, Respiratory mechanics in rabbits ventilated with different tidal volumes, *Respiration Physiology* **106** (1996) pp. 307–316.
[32] A. F. M. Verbraak, J. M. Bogaard, J. E. W. Beneken, E. Hoorn and A. Versprille. Serial lung model for simulation and parameter estimation in body plethysmography, *Med. Biol. Eng. Comput.* **29** (1991) pp. 309–317.